Published in final edited form as:
*Brain Stimul*. 2009 October 1; 2(4): 201–207. doi:10.1016/j.brs.2009.03.005.

# Gyri –precise head model of transcranial DC stimulation: Improved spatial focality using a ring electrode versus conventional rectangular pad

**Abhishek Datta**, **Varun Bansal**, **Julian Diaz**, **Jinal Patel**, **Davide Reato**, and **Marom Bikson***
The City College of the City University of New York, New York, NY

## Abstract

The spatial resolution of conventional transcranial direct current stimulation (tDCS) is considered to be relatively diffuse owing to skull dispersion. However, here we show that electric fields may be clustered at distinct gyri/sulci sites due to details in tissue architecture/conductivity notably cerebrospinal fluid (CSF). We calculated the cortical electric field/current density magnitude induced during tDCS using a high spatial resolution (1 $mm^3$) MRI-derived finite element human head model; cortical gyri/sulci were resolved. The spatial focality of conventional rectangular-pad (7 × 5 $cm^2$) and the ring (4 × 1) electrode configurations were compared. The rectangular-pad configuration resulted in diffuse (un-focal) modulation, with discrete clusters of electric field magnitude maxima. Peak induced electric field magnitude was not observed directly underneath the pads, but at an intermediate lobe. The 4 × 1 ring resulted in enhanced spatial focality, with peak induced electric field magnitude at the sulcus and adjacent gyri directly underneath the active electrode. Cortical structures may be focally targeted using ring configurations. Anatomically accurate high resolution MRI-based forward-models may guide the 'rational' clinical design and optimization of tDCS.

### Keywords

tDCS; focality; Finite Element Modeling; MRI Human Head Model; TES

## Introduction

Conventional transcranial direct current stimulation (tDCS) involves weak direct currents (260 μA – 2 mA) applied to the scalp via sponge-based rectangular pads (nominally 25 - 35 $cm^2$) (1–4). tDCS modulates cortical function and has been applied to facilitate learning, alter behavioral performance, and improve impaired brain function (5–13).

A pivotal factor for tDCS efficacy and safety is the spatial extent of induced cortical electric fields/current density. tDCS is considered to be poorly focused using rectangular-pad electrode configurations (14–17). The spatial focality of induced cortical electric field (EF)/ current densities has been proposed to increase using reduced electrode sizes (16–18),



*T-403 B Steinman Hall, Grove School of Engineering, The City College of the CUNY, 160 Convent Avenue, New York, NY 10031, bikson@ccny.cuny.edu.

appropriate placement of electrodes (15,17,19), and ring electrode configurations (17). However, the precise role of complex tissue-compartment morphology in influencing the flow of currents during tDCS has not been systematically addressed, including potential discrete cortical “hotspots” (clustering) of induced electric fields (20–22).

During any transcranial current stimulation modality, the current which reaches the cortex is significantly altered from the applied scalp current due to intermediate tissue properties. A portion of the injected current is shunted across the scalp. The portion which crosses into the skull is then conducted by cerebrospinal fluid (CSF). Through the highly conductive CSF network, current can eventually cross into the brain. In the case of DC stimulation, induced cortical currents / electric fields have been shown to modulate the firing properties of neurons and ‘condition’ neuronal excitability (23–27). There is a general perception that the low conductivity of skull places a severe limit on the spatial focality of brain modulation.

One objective of this paper was to compare the focality of ‘conventional’ $7 \times 5$ cm$^2$ rectangular-pad stimulation with the $4 \times 1$ ring electrode configuration using a high resolution MRI-based finite element model of the human head. Spherical-based (17,21) and MRI-derived (22,28) head models have previously been used to calculate tDCS electric fields. In this study, we incorporated gyri/sulci specificity by developing a model with 1 mm$^3$ resolution. Induced cortical electric fields were used to predict relative spatial focality and the influence of tissue geometry/conductivity. We report that tDCS modulation maps are fundamentally influenced by detailed cortical architecture and consider limitations on transcranial stimulation focality

## Methods

Volume conductor models were created with the same resolution (1 mm$^3$) as the MRI data used to derive them. Raw 3T MRI scans were contrast enhanced and noise filtered. The head was segmented into compartments representing the brain tissue, cerebrospinal fluid (CSF), skull, muscle, fatty tissue, eyes, blood vessels and the scalp respectively (Figure 1 A; SIMPLEWARE Ltd., Exeter, UK). The stimulation rectangular pads and discs were imported as CAD models (see below). The volumetric mesh was generated (minimum quality factor > 0.5) from the segmented data and eventually exported to COMSOL Multiphysics 3.4 (COMSOL Inc., MA, USA). The resulting mesh comprised >10,000,000 tetrahedral elements (>15,000,000 degrees of freedom).

The electrical properties of the tissues were assigned representative isotropic average values (in S/m): brain: 0.2; CSF: 1.65; skull: 0.01; scalp: 0.465 (29–36). The muscle, fatty tissue, eyes and blood vessel compartments were assigned the conductivity of scalp tissue.

We modeled two electrode configurations:

1. ‘Rectangular-pad’ (Figure 1B): Two pads ($7 \times 5$ cm$^2$) were placed at sites commonly used for tDCS of the primary motor cortex, with the “active” (anode) electrode over the left motor cortex and the “return” (cathode) electrode at the forehead above the contralateral orbita. Typically, the rectangular sponges are soaked in saline for conventional tDCS application and the abutting electrode is energized. The sponge was therefore assigned the conductivity of saline: 1.4 S/m.
2. ‘$4 \times 1$ ring’ (Figure 1C): In order to practically implement the concentric-ring configuration (17), we approximated a ring using four “return” (cathode) disc electrodes arranged in a circular fashion around an “active” (anode) center electrode. The active electrode is placed over the motor cortex (coinciding with the center of the active pad used for rectangular-pad stimulation) and surrounded by

four return electrodes (each at a disc center to disc center distance of 3 cm from the active electrode). The disc electrodes had a 4 mm radius. The 4 × 1 ring electrode system was implemented by passing current through disc electrodes into the scalp using a customized tDCS gel (CCNY-4) with conductivity: 0.3 S/m.

All electrodes had a thickness of ~ 1 mm and were modeled as conductors with the conductivity of copper: $5.8 \times 10^7$ S/m. The thickness of the CCNY-4 gel was ~ 2 mm while the thickness of the sponge varied from 1 to 2.5 mm (thickness changed with scalp curvature in order to maintain continuous contact).

The Laplace equation $\nabla.(\sigma \nabla V) = 0$ (V: potential; $\sigma$: conductivity) was solved and the boundary conditions used were (1) inward current flow = $J_n$ (normal current density) applied to the exposed surface of the anode electrode, (2) ground applied to the exposed surface of the cathode electrode(s) and (3) all other external surfaces treated as insulated. Current densities corresponding to 1 mA total current for the rectangular-pad configuration and 2 mA total current for the 4 × 1 ring configuration were respectively applied. These currents resulted in similar peak cortical induced EF magnitude for each of the configurations. The finite element method (FEM) model was implemented using COMSOL. The linear system solver of conjugate gradients was used with a relative tolerance of $1 \times 10^{-6}$.

'Surface-magnitude' plots were generated by plotting the magnitude of EF on the surface of brain tissue. In addition, 'Cross-section magnitude' plots were generated by plotting the EF magnitude on coronal slices (17). Because the conductivity of brain is uniform, these same plots also represent induced current density profiles (where the actual current density values can be scaled using: $J = \sigma.E$).

In this study, the induced brain electric field magnitude was assumed to correlate with the degree of brain "modulation". The consideration of the electric field (as opposed to the classical activating function) may be appropriate if: 1) tDCS induced electric fields are uniform at the scale of a neuron; and 2) neuronal modulation may be directly correlated with uniform electric field magnitude (17, 26, 37–41). Our electric field magnitude modulation maps do not consider any specific neuronal orientation (and target non-oriented structures) (17, 42).

## Results

For the 7 × 5 $cm^2$ rectangular-pad and the 4 × 1 ring configuration models (Figure 1B and Figure 1C), we calculated the induced electric field/current density magnitude in the brain. The surface-magnitude/cross-section magnitude EF plots for each of the configurations allow a direct comparison of relative cortical surface and depth focality (Figure 2).

Rectangular-pad stimulation with 7 × 5 $cm^2$ pads results in widespread diffuse (un-focal) modulation over the entire cortical surface owing to the large size and separation of pads (Figure 2A.2). 1 mA injected through the pads results in 0.67 V/m peak cortical EF magnitude (encompassed in dashed region of Figure 2A.2; expanded in Figure 2A.4) in the walls of a frontal lobe gyrus. The peak cortical EF magnitude of 0.67 V/m corresponds to 0.13 $A/m^2$ peak cortical current density magnitude. The local EF magnitude peak directly underneath the pads was 0.45 V/m. The minimum cortical induced EF magnitude in the entire frontal area of the brain was ~ 0.16 V/m (see coronal slice, Figure 2A.6) and ~ 0.06 V/m in the occipital area.

The presence of distinct clusters of EF magnitude maxima (Figure 2A.2) was influenced by regions of reduced skull thickness, which may provide preferential current pathways of current crossing into the CSF (see also Supplementary Figure), as well as channels of high-

conductivity CSF bounded by brain and skull. For example, a particular gyrus may have high induced EF magnitude due to wide pockets of CSF on either side acting as a current "sink" (36) as well as reduced CSF thickness over that gyri crown acting as a "funnel".

The 4 × 1 ring configuration leads to a significant increase in spatial focality (Figure 2B.2). Peak electric field magnitude is observed in the gyri and the intermediate sulcus directly underneath the active stimulation electrode (see coronal slice, Figure 2B.6). The region of modulation is generally constrained between the active electrode and the four return electrodes with a 0.44 V/m EF magnitude peak (encompassed in dashed region of Figure 2B.2; expanded in Figure 2B.4). Thus, using the 4 × 1 ring configuration, 2 mA resulted in a comparable peak EF magnitude in the motor cortex as 1 mA rectangular-pad (7 × 5 $cm^2$) stimulation. However, for the 4 × 1 ring configuration, there was no cortical modulation (< 0.01 V/m) in the frontal regions, on the contralateral (right) motor regions of the brain, or on the occipital lobe of the brain. The overall spatial profile of brain modulation was strongly influenced by tissue inhomogeneity, notably due to CSF (Supplementary Figure).

## Discussion

The translation of stimulation models to clinical applications requires reproducing application-appropriate anatomical features (43–50). The incorporation of gyri/ sulci specificity in our 3D human head model can guide rational tDCS design and optimization (42, 51).

The overall current flow due to any transcranial electric stimulation is complex and is influenced by a convergence of factors including: 1) electrode size/geometry and separation-distance, with related scalp shunting (17); 2) skull thickness, presence of sutures and eye cavities; 3) channels of high conductivity CSF enclosing/and perfusing the underlying cortex; 4) convoluted brain surface morphology; and 5) differences in tissue conductivities at boundaries between tissue compartments.

tDCS using conventional 'large' rectangular pads resulted in diffuse (un-focal) cortical modulation. Moreover, the complex geometry of the brain and regional differences in conductance cause local non-uniformities of current density through the CSF (e.g. "sinks" and "funnels") that are reflected in clustering of brain electric field magnitude at distinct sites. Indeed, some imaging and physiological studies suggest diffuse brain modulation and clustering of regional cerebral blood flow/EF, independent of anatomical connections (20,52). Separate imaging, TMS mapping studies and, clinical studies indicate some level of functional spatial selectivity (1, 5, 7–9); which may be explained by FE models with more specific modulation maps (17) including non-linearities and thresholding.

Whereas our electric-field magnitude modulation maps assume no particular neuronal geometry or waveform dependent biophysical transduction mechanisms, direction-specific modulation maps incorporating cellular orientation (radial versus tangential) (17) and electric field derivative (classical activating function) (53,54) have been applied elsewhere (43,44,47). In cases of pulsed or AC stimulation waveforms, the appropriate modulation map (parameter/function that determines degree of brain "modulation") may differ (20, 55, 56).

Any FE human head model is limited by the accuracy of tissue dimensions and conductivity values incorporated (inhomogeneity and anisotropy). The present study investigated the distribution of tDCS induced currents in brain using a highly detailed anatomical model. The high MRI scan resolution (1 $mm^3$) allows accurate segmentation of individual tissue compartments. Consequently the precise 3D model rendered, captures anatomical detail such as cortical folding (Figure 2.A.4). Finally the precise FE mesh generated (> 10 million

elements), allows accurate computation of induced fields. The importance of incorporating gyri/sulci specificity is highlighted by the observance of clustering of brain modulation during conventional tDCS (see also Supplementary Figure). Our results also suggest that individual variability would affect the magnitude and spatial extent of cortical electric fields. For example, young children have vascularized fontanels, there are differences in the degree/timing of suture closing amongst adults (36), and elderly subjects have larger fractional CSF volumes (57).

Our results indicate that the focality of clinical tDCS application can be significantly enhanced by the 4 × 1 ring configuration. Additionally, since the peak induced cortical electric field magnitude is similar to the rectangular-pad stimulation; the 4 × 1 ring results in more targeted brain modulation (hence potentially, a safer electrode configuration). The cortical current density of 0.09 $A/m^2$ induced underneath the pads by rectangular pad (1 mA) and 4 × 1 ring (2 mA) configurations is more than two orders of magnitude away from the threshold for histopathologically observed tDCS brain damage in a rat model (58). We emphasize that using the 4 × 1 ring configuration, the more *surface* current needed does not lead to more peak induced cortical EF magnitude, but reflects shunting across the scalp (without crossing into the brain).

For skin safety, the increased scalp current associated with 4 × 1 ring can be offset by increasing the separation distance between stimulation electrodes, but at the cost of stimulation focality (17). Importantly when using conventional sponge electrodes, the current density at the scalp is in fact concentrated at the sponge edges and thus exceeds the average current density (injected current / electrode surface area) (21,22). Moreover, electrode materials and design are as pivotal to comfort as is average current density (59–61); using appropriate hardware (electrode adapters, stimulation gels), 39.8 $A/m^2$ current density may be applied without pain (62). Because of the above issues, pain perception for skin should be addressed in a clinical study (63). Thus electrode designs that mitigate skin irritation should be developed along with electrode configurations that enhance spatial focality.

The quasi-static field approximation implies conservation and linearity of EF solution. Thus, our EF magnitude ‘spatial profile’ results can be extrapolated to other transcranial current stimulation modalities (e.g. suprathreshold transcranial electrical stimulation, electroconvulsive therapy, transcranial alternating current stimulation, transcranial random noise stimulation, and cranial electrotherapy stimulation) (20,55,56,64,65) where the 4 × 1 ring configuration may be used to focally target cortical structures.

The ‘transparency’ of the skull to magnetic stimulation has led to the development of specialized coils for focused transcranial stimulation (50,66–69). There is a general perception that the low conductivity of skull places a severe limit on spatial focality of electrical stimulation. The results of this modeling study support the further development of transcranial current stimulation technology for focal stimulation.

## Supplementary Material

Refer to Web version on PubMed Central for supplementary material.

## Acknowledgments

Ross Cotton of SIMPLEWARE Ltd. and Konrad Juethner of COMSOL Inc. The authors also wish to thank Pejman Sehatpour at Nathan Kline Institute; Thomas Radman, Fortunato Battaglia, and Lucas Parra of the City College of New York. This work was supported by NIH (41341-23, 41595-00), Andy Grove Foundation, and PSC-CUNY grants.

## References


1. Nitsche MA, Paulus W. Excitability changes induced in the human motor cortex by weak transcranial direct current stimulation. J Physiol. 2000; 527:633–639. [PubMed: 10990547]
2. Marshall L, Molle M, Siebner HR, Born J. Bifrontal transcranial direct current stimulation slows reaction time in a working memory task. BMC Neurosci. 2005; 6:23. [PubMed: 15819988]
3. Iyer MB, Mattu U, Graffman J, et al. Safety and cognitive effect of frontal DC brain polarization in healthy individuals. Neurology. 2005; 64:872–875. [PubMed: 15753425]
4. Hummel F, Celnik P, Giraux P, et al. Effects of non-invasive cortical stimulation on skilled motor function in chronic stroke. Brain. 2005; 128:490–499. [PubMed: 15634731]
5. Nitsche MA, Schauenburg A, Lang N, et al. Facilitation of implicit motor learning by weak transcranial direct current stimulation of the primary motor cortex in the human. J Cogn Neurosci. 2003; 15:619–626. [PubMed: 12803972]
6. Uy J, Ridding MC. Increased cortical excitability induced by transcranial DC and peripheral nerve stimulation. J Meurosci Methods. 2003; 127:193–197.
7. Kincses TZ, Antal A, Nitsche MA, Bartfai O, Paulus W. Facilitation of probabilistic classification learning by transcranial direct current stimulation of the prefrontal cortex in the human. Neuropsychologia. 2004; 42:113–117. [PubMed: 14615081]
8. Antal A, Kincses TZ, Nitsche MA, Bartfai O, Paulus W. Excitability changes induced in the human primary visual cortex by transcranial direct current stimulation: direct electrophysiological evidence. Invest Ophthalmol Vis Sci. 2004; 45(2):702–707. [PubMed: 14744917]
9. Boggio PS, Bermpohl F, Vergara AO, et al. Go-no-go task performance improvement after anodal transcranial DC stimulation of the left dorsolateral prefrontal cortex in major depression. J Affect Disord. 2006; 101:91–98. [PubMed: 17166593]
10. Liebetanz D, Klinker F, Hering D, et al. Anticonvulsant effects of transcranial direct-current stimulation (tDCS) in the rat cortical ramp model of focal epilepsy. Epilepsia. 2006; 47:1216–1224. [PubMed: 16886986]
11. Boggio PS, Ferrucci R, Rigonatti SP, et al. Effects of transcranial direct current stimulation on working memory in patients with Parkinson's disease. J Neurol Sci. 2006; 249:31–38. [PubMed: 16843494]
12. Fregni F, Boggio PS, Lima MC, et al. A sham-controlled, phase II trial of transcranial direct current stimulation for the treatment of central pain in traumatic spinal cord injury. Pain. 2006; 122:197–209. [PubMed: 16564618]
13. Boggio PS, Khoury LP, Martins DC, et al. Temporal cortex DC stimulation enhances performance on a visual recognition memory task in Alzheimer's disease. J Neurol Neurosurg Psychiatry. 2008 Epub.
14. Rossini PM, Marciani MG, Caamia M, Roma V, Zarola F. Nervous propagation along 'central' motor pathways in intact man: characteristics of motor responses to 'bifocal' and 'unifocal' spine and scalp non-invasive stimulation. Electroencephalogr Clin Neurophysiol. 1985; 61:272–286. [PubMed: 2411506]
15. Nathan SS, Sinha SR, Gordon B, Lesser RP, Thakor NV. Determination of current density distributions generated by electrical stimulation of the human cerebral cortex. Electroencephalogr Clin Neurophysiol. 1993; 86:183–192. [PubMed: 7680994]
16. Nitsche MA, Doemkes S, Karakose T, et al. Shaping the effects of transcranial direct current stimulation of the human motor cortex. J Neurophysiol. 2007; 97:3109–3117. [PubMed: 17251360]
17. Datta A, Elwassif M, Battaglia F, Bikson M. Transcranial current stimulation focality using disc and ring electrode configurations: FEM analysis. J Neural Eng. 2008; 5:163–174. [PubMed: 18441418]
18. Kwon YH, Ko MH, Ahn SH, et al. Primary motor cortex activation by transcranial direct current stimulation in the human brain. Neurosci Lett. 2008; 435:56–59. [PubMed: 18325666]
19. Borckardt JJ, Linder KJ, Ricci R, et al. Focal electrically administered therapy: device parameter effects on stimulus perception in humans. J ECT. 2008 [Epub].

20. Kanai R, Chaieb L, Antal A, Walsh V, Paulus W. Frequency-dependent electrical stimulation of the visual cortex. Curr Biol. 2008; 18(23):1839–1843. [PubMed: 19026538]
21. Miranda PC, Lomarev M, Hallett M. Modeling the current distribution during transcranial direct current stimulation. Clin Neurophysiol. 2006; 117:1623–1629. [PubMed: 16762592]
22. Wagner T, Fregni F, Fecteau S, et al. Transcranial direct current stimulation: a computer based human model study. Neuroimage. 2007; 35:1113–1124. [PubMed: 17337213]
23. Purpura DP, McMurty JG. Intracellular activities and evoked potential changes during polarization of motor cortex. J Neurophysiol. 1965; 28:166–185. [PubMed: 14244793]
24. Bindman LJ, Lippold OCJ, Redfearn JWT. The action of brief polarizing currents on the cerebral cortex of the rat (1) during current flow and (2) in the production of long-lasting after-effects. J Physiol. 1964; 172:369–382. [PubMed: 14199369]
25. Gartside IB. Mechanisms of sustained increases of firing rate of neurons in the rat cerebral cortex after polarization: role of protein synthesis. Nature. 1968; 220:383–384. [PubMed: 4300961]
26. Bikson M, Inoue M, Akiyama H, et al. Effects of uniform extracellular DC electric fields on excitability in rat hippocampal slices in vitro. J Physiol. 2004; 557:175–190. [PubMed: 14978199]
27. Radman T, Su Y, An JH, Parra LC, Bikson M. Spike timing amplifies the effect of electric fields on neurons: implications for endogenous field effects. J Neurosci. 2007; 27:3030–3036. [PubMed: 17360926]
28. Oostendorp, TF.; Hengeveld, YA.; Wolters, CH., et al. Modeling Transcranial DC Stimulation; Conf Proc IEEE Eng Med Biol Soc; 20–25 Aug; 2008. p. 4226-4229.
29. Geddes LA, Baker LE. The specific resistance of biological material-a compendium of data for the biomedical engineer and physiologist. Med Biol Eng. 1967; 5:271–293. [PubMed: 6068939]
30. Akhtari M, Bryant HC, Mamelak AN, et al. Conductivities of a three-layer live human skull. Brain Topogr. 2002; 14(3):151–167. [PubMed: 12002346]
31. Ranck JB. Specific impedance of rabbit cerebral cortex. Exp Neurol. 1963; 7:144–152. [PubMed: 13990734]
32. Baumann SB, Wozny DR, Kelly SK, Meno FM. The electrical conductivity of human cerebrospinal fluid at body temperature. IEEE Trans Biomed Eng. 1997; 44(3):220–223. [PubMed: 9216137]
33. Gabriel C, Gabriel S, Corthout E. The dielectric properties of biological tissues: I. Literature survey. Phys Med Biol. 1996; 41(11):2231–2249. [PubMed: 8938024]
34. Hauesien J, Ramon C, Eiselt M, Brauer H, Nowak H. Influence of tissue resistivities on neuromagnetic fields and electric potentials studied with a finite element model of the head. IEEE Trans Biomed Eng. 1997; 44(8):727–735. [PubMed: 9254986]
35. Nadeem M, Thorlin T, Gandhi OP, Persson M. Computation of electric and magnetic stimulation in human head using the 3-D impedance method. IEEE Trans Biomed Eng. 2003; 50:900–907. [PubMed: 12848358]
36. Holdefer RN, Sadleir R, Russell MJ. Predicted current densities in the brain using transcranial electrical stimulation. Clin Neurophysiol. 2006; 117:1388–1397. [PubMed: 16644273]
37. Tranchina D, Nicholson C. A model for the polarization of neurons by extrinsically applied electric fields. J Biophys. 1986; 50:1139–1156.
38. Nagarajan SS, Durand DM, Warman EN. Effects of induced electric fields on finite neuronal structures: a simulation study. IEEE Trans Biomed Eng. 1993; 40:1175–1188. [PubMed: 8307602]
39. Amassian VE, Eberle L, Maccabee PJ, Cracco RQ. Modelling magnetic coil excitation of human cerebral cortex with a peripheral nerve immersed in a brain-shaped volume conductor: the significance of fibre bending in excitation. Electroencephalogr Clin Neurophysiol. 1992; 85:291–301. [PubMed: 1385089]
40. Roth BJ. Mechanisms for electrical stimulation of excitable tissue. Crit Rev Biomed Eng. 1994; 22:253–305. [PubMed: 8598130]
41. Chan CY, Nicholson C. Modulation by applied electric fields of purkinje and stellate cell activity in the isolated turtle-cerebellum. J Physiol. 1986; 371:89–114. [PubMed: 3701658]

42. Bikson M, Bulow P, Stiller JW, et al. Transcranial direct current stimulation for major depression: a general system for quantifying transcranial electrotherapy dosage. Curr Treat Options Neurol. 2008; 10(5):377–385. [PubMed: 18782510]
43. Johnson MD, McIntyre CC. Quantifying the neural elements activated and inhibited by global pallidus deep brain stimulation. 2008; 100(5):2549–2563.
44. Wongsarnpigoon A, Grill WM. Computational modeling of epidural cortical stimulation. J Neural Eng. 2008; 5(4):443–454. [PubMed: 19015584]
45. Im CH, Jung HH, Choi JD, Lee SY, Jung KY. Determination of optimal electrode positions for transcranial direct current stimulation (tDCS). Phys Med Biol. 2008; 53:219–225.
46. Manola L, Holsheimer J, Veltink P, Buitenweg JR. Anodal vs cathodal stimulation of motor cortex: a modeling study. Clin Neurophysiol. 2007; 118:464–474. [PubMed: 17150409]
47. Butson CR, Cooper SE, Henderson JM, McIntyre CC. Patient-specific analysis of the volume of tissue activated during deep brain stimulation. Neuroimage. 2007; 34(2):661–670. [PubMed: 17113789]
48. Holsheimer J. Computer modelling of spinal cord stimulation and its contribution to therapeutic efficacy. Spinal Cord. 1998; 36(8):531–540. [PubMed: 9713921]
49. De Lucia M, Parker GJM, Embleton K, Newton JM, Walsh V. Diffusion tensor MRI-based estimation of the influence of brain tissue anisotropy on the effects of transcranial magnetic stimulation. Neuroimage. 2007; 36:1159–1170. [PubMed: 17524673]
50. Deng, ZD.; Peterchev, AV.; Lisanby, SH. Coil design considerations for deep-brain transcranial magnetic stimulation (dTMS); Conf Proc IEEE Eng Med Biol Soc; 20–25 Aug; 2008. p. 5675-5679.
51. Bikson, M.; Radman, T.; Datta, A. Rational modulation of neuronal processing with applied electric fields; Conf Proc IEEE Eng Med Biol Soc; 2006. p. 1616-1619.
52. Lang N, Siebner HR, Ward NS, et al. How does transcranial DC stimulation of the primary motor cortex alter regional neuronal activity in the human brain? Eur J Neurosci. 2005; 22:495–504. [PubMed: 16045502]
53. Rattay F. Analysis of models for external stimulation of axons. IEEE Trans Biomed Eng. 1986; 33:974–977. [PubMed: 3770787]
54. Plonsey R, Barr RC. Electric field stimulation of excitable tissue. IEEE Trans Biomed Eng. 1995; 42:329–336. [PubMed: 7729832]
55. Terney D, Chaieb L, Moliadze V, Antal A, Paulus W. Increasing human brain excitability by transcranial high frequency random noise stimulation. J Neurosci. 2008; 28(53)
56. Lisanby SH. Electroconvulsive therapy for depression. N Eng J Med. 2007; 357:1939–1945.
57. Murphy DG, DeCarli C, Schapiro MB, Rapoport SI, Horwitz B. Age-related differences in volumes of subcortical nuclei, brain matter, and cerebrospinal fluid in healthy men as measured with magnetic resonance imaging. Arch Neurol. 1992; 49(8):839–845. [PubMed: 1343082]
58. Liebetanz D, Koch R, Mayenfels S, et al. Safety limits of cathodal transcranial direct current stimulation in rats. Clin Neurophysiol. 2009 “In Press”.
59. Dundas JE, Thickbroom GW, Mastaglia FL. Perception of comfort during transcranial direct current stimulation: effect of NaCl solution concentration applied to sponge electrodes. Clin Neurophysiol. 2007; 118:1166–1170. [PubMed: 17329167]
60. Palm U, Keeser D, Schiller C, et al. Skin lesions after treatment with transcranial direct current stimulation (tDCS). Brain Stimulation. 2008; 1:386–387. [PubMed: 20633396]
61. Merrill DR, Bikson M, Jefferys JG. Electrical stimulation of excitable tissue: design of efficacious and safe protocols. J Neurosci Methods. 2005; 141:171–198. [PubMed: 15661300]
62. Prausnitz MR. The effects of electric current applied to skin: A review for transdermal drug delivery. Advanced Drug Delivery Reviews. 1996; 18:395–425.
63. Arana AB, Borckardt JJ, Ricci R, et al. Focal electrical stimulation as a sham control for repetitive transcranial magnetic stimulation: does it truly mimic the cutaneous sensation and pain of active prefrontal repetitive transcranial magnetic stimulation? Brain Stimulation. 2008; 1:44–51. [PubMed: 19424459]

64. Calancie B, Harris W, Broton JG, Alexeeva N, Green BA. 'Threshold-level' multipulse transcranial electrical stimulation of motor cortex for intraoperative monitoring of spinal motor tracts: description of method and comparison to somatosensory evoked potential monitoring. J Neurosurg. 1998; 88:457–470. [PubMed: 9488299]

65. Schroeder MJ, Barr RE. Quantitative analysis of the electroencephalogram during cranial electrotherapy stimulation. Clin Neurophysiol. 2001; 112:2075–2083. [PubMed: 11682346]

66. Cohen LG, Roth BJ, Nilsson J, et al. Effects of coil design on delivery of focal magnetic stimulation. Technical considerations. Electroencephalogr Clin Neurophysiol. 1990; 75:350–357. [PubMed: 1691084]

67. Ren C, Tarjan PP, Popovic DB. A novel electric design for electromagnetic stimulation - The slinky coil. IEEE Trans Biomed Eng. 1995; 42:918–925. [PubMed: 7558066]

68. Ruohonen J, Ilmoniemi RJ. Focusing and targeting brain stimulation using multiple coils. Med Biol Eng Comput. 1998; 36:297–301. [PubMed: 9747568]

69. Roth Y, Zangen A, Hallett M. A coil design for transcranial magnetic stimulation of deep brain regions. J Clin Neurophysiol. 2002; 19:361–370. [PubMed: 12436090]

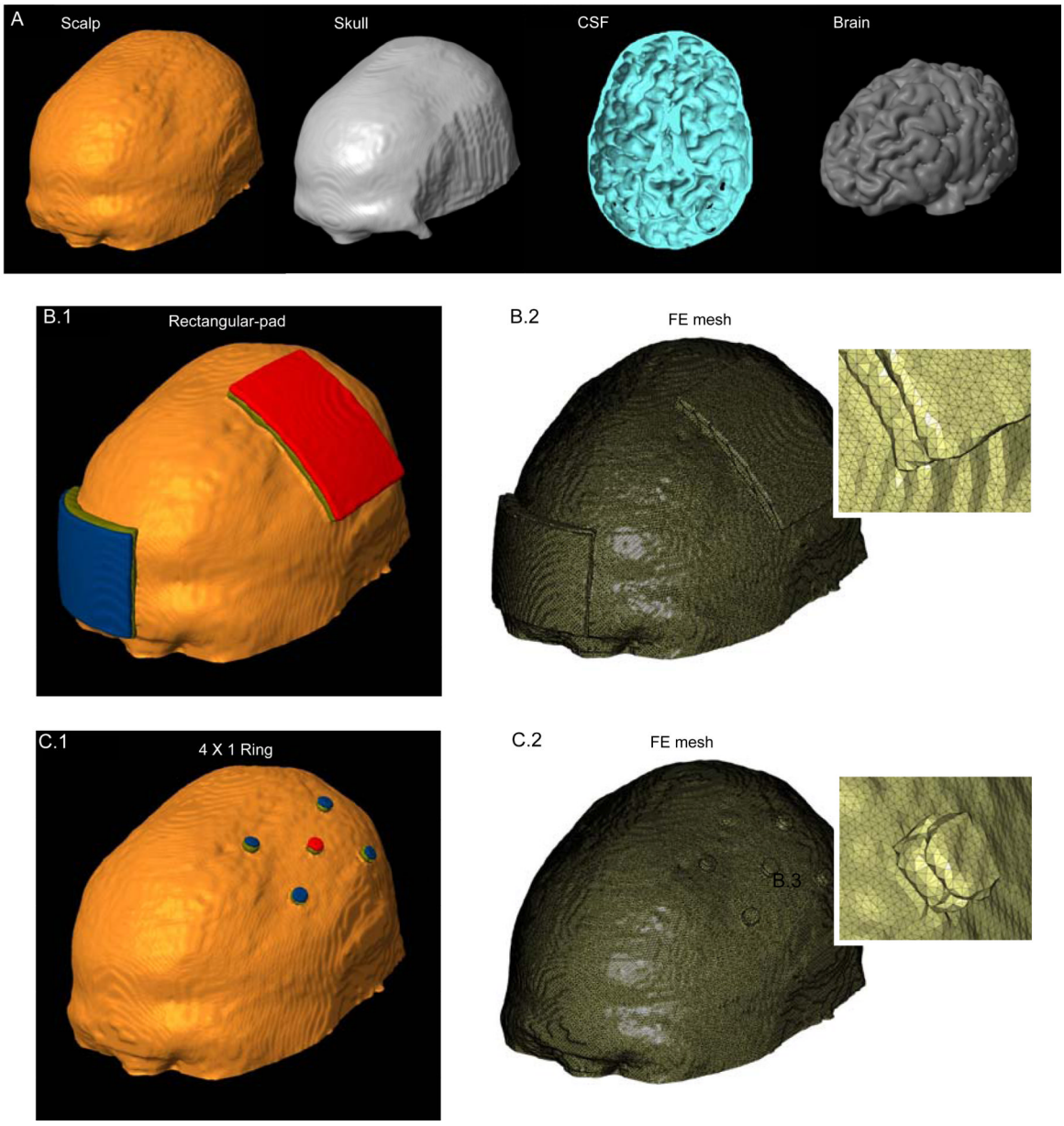


**Figure 1.**

Finite element (FE) model of the conventional 7 × 5 $cm^2$ rectangular-pad and 4 × 1 ring configurations. (A) Segmented compartments in the following order: Scalp, Skull, CSF and Brain. (B.1) FE model of the conventional rectangular-pad configuration and corresponding FE mesh (B.2). (C.1) FE model of the 4 × 1 ring electrode configuration and corresponding FE mesh (C.2). The two insets show the zoomed mesh images, highlighting finer detail. 'Red': Anode electrode; 'Blue': Cathode electrode(s); 'Olive green': sponge/gel.

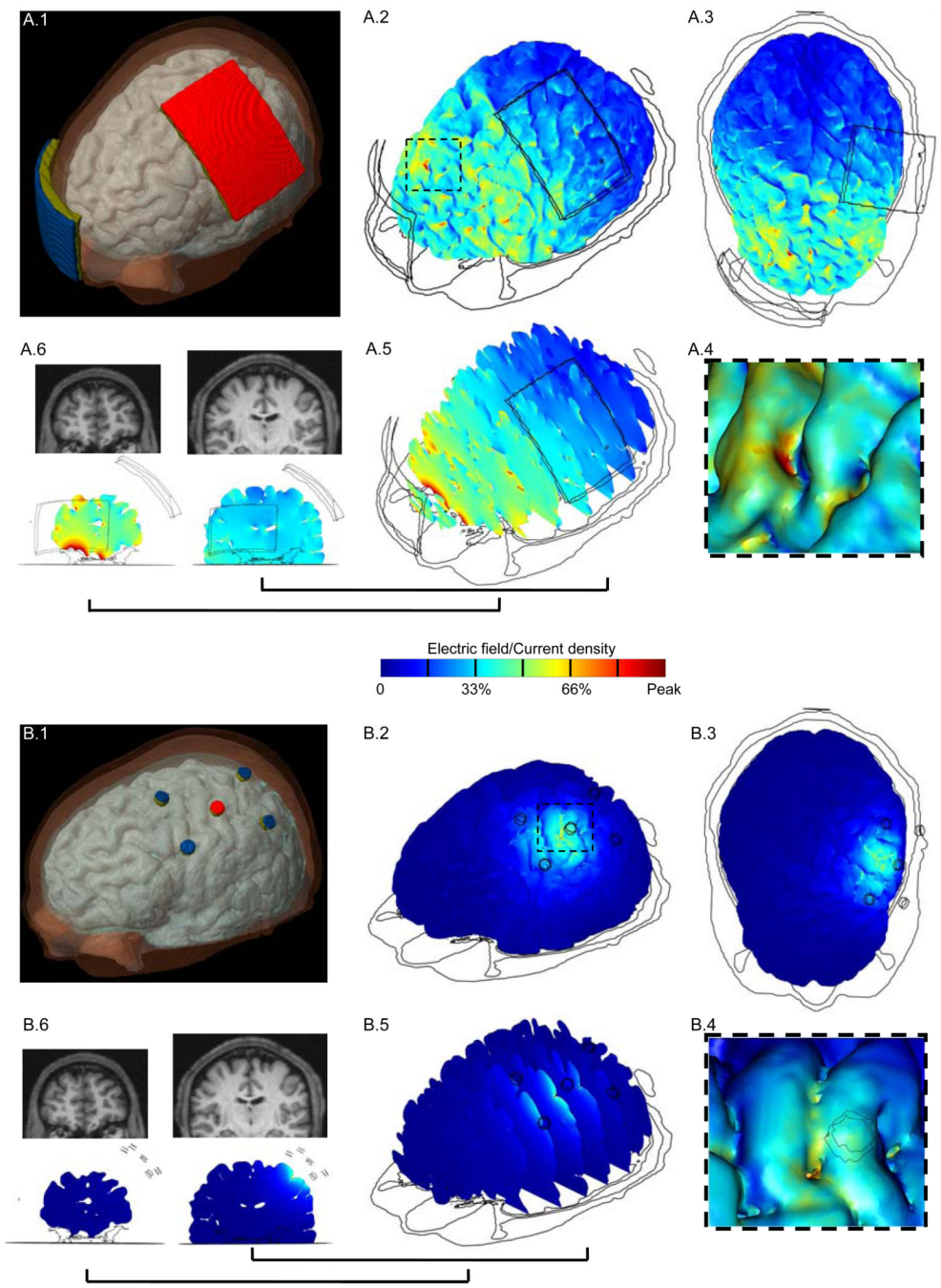


**Figure 2.**

Brain modulation during tDCS using conventional rectangular-pad (A.1) and the 4 × 1 ring electrode configuration (B.1). 'Red': Anode electrode; 'Blue': Cathode electrode(s); 'Olive green': sponge/gel. For each configuration, we calculated the induced cortical electric field (EF) magnitude. (A.2, B.2) *Surface-magnitude* plots of EF along the brain surface, same view as (A.1, B.1). The dashed region is expanded in inset. (A.3, B.3) *Top view* of the brain showing the induced *surface-magnitude* EF. The insets (A.4) and (B.4) show the zoomed *surface-magnitude* EF plots. These images are obtained with "lighting" on [COMSOL Multiphysics] to highlight gyri/sulci modulation. (A.5, B.5) *Cross-section magnitude* EF plotted on a series of successive cortical slices, same view as (A.1, B.1). The *cross-section*

*magnitude* EF plots for two slices and their corresponding MRI scans are shown in (A.6), (B.6). One slice is chosen directly from underneath the rectangular-pad/active electrode of 4 × 1 ring configuration and another from the prefrontal area of the brain. The same slices are shown for each of the configurations. All plots are normalized between zero and the peak positive cortical EF magnitude: conventional rectangular-pad peak = 0.67 V/m (or 0.13 A/$m^2$ current density peak); 4 × 1 ring peak = 0.44 V/m. (Note that for the rectangular-pad, the EF magnitude peak is observed between the pads and not underneath).